**THE EUROPEAN
PHYSICAL JOURNAL C**

NLO photon parton parametrization using ee and ep data[*]

W. Slominski[1,a], H. Abramowicz[2,b], A. Levy[2]

[1] M. Smoluchowski Institute of Physics, Jagellonian University, Reymonta 4, 30-059 Cracow, Poland
[2] School of Physics and Astronomy, Raymond and Beverly Sackler Faculty of Exact Sciences, Tel-Aviv University, Tel-Aviv, Israel

Abstract. An NLO photon parton parametrization is presented based on the existing F_2^γ measurements from e^+e^- data and the low-x proton structure function from ep interactions. Also included in the extraction of the NLO parton distribution functions are the dijets data coming from $\gamma p \to j_1 + j_2 + X$. The new parametrization is compared to other NLO parametrizations.

1 Introduction

In spite of the photon being a fundamental gauge particle of electromagnetic interactions, it is known to develop a hadronic structure in its interactions with matter. The notion of the hadronic structure function of the photon, F_2^γ, is introduced in analogy to the well known nucleon case. The first measurements of F_2^γ became available from e^+e^- collisions in which one of the leptons is scattered under a small angle. These interactions may then be interpreted as processes in which a highly virtual photon, of virtuality Q^2, probes an almost real target photon, with virtuality $P^2 \approx 0$.

While the proton structure function F_2^p has been well measured over a wide range of Q^2 and the Bjorken variable x [1], F_2^γ data cover a restricted kinematic range $(0.001 < x < 0.9)$ and are subject to much larger systematic uncertainties [2]. This is mainly due to experimental limitations in measuring the centre of mass energy W of the $\gamma^*\gamma$ system, in particular at large values of W.

In the present paper, a new parametrization of the parton distributions in the photon is extracted in next-to-leading order (NLO) of perturbative QCD. It differs from other NLO parametrizations [3–7] in that the data used in the fitting procedure include the expected behaviour of F_2^γ at low-x [8], as derived from F_2^p measurements [9] under Gribov factorization assumption [10] and, in addition, the measurements of the dijet photoproduction cross sections [11].

2 Theoretical background

2.1 Physical quantities and parton distributions

In QCD, the hadronic cross sections are given as convolutions of coefficient functions and parton densities. In higher

orders of perturbative expansion, the definition of parton densities is not unique and depends on the adopted factorization scheme. In this paper we adopt the DISγ factorization scheme [3], where the relation between F_2^γ and the parton distributions, $f_k^\gamma(x, Q^2)$ ($k = q$ or G), is given by

$$\bar{F}_2^\gamma(Q^2) = \left[1 + \frac{\alpha_s(Q^2)}{2\pi} C_{F,2}^{(1)}\right] \otimes \sum_{q=1}^{N_f} 2e_q^2 f_q^\gamma(Q^2)$$
$$+ \left(\sum_{q=1}^{N_f} e_q^2\right) \frac{\alpha_s(Q^2)}{2\pi} C_{G,2}^{(1)} \otimes f_G^\gamma(Q^2), \quad (1)$$

where $\bar{F}_2^\gamma(x, Q^2) \equiv \frac{1}{x} F_2^\gamma(x, Q^2)$, $\alpha_s(Q^2)$ is the QCD running coupling constant, $\otimes$ denotes convolution, N_f is the number of flavours and e_q is the electric charge of quark q in units of e. The parton distributions are convoluted with known coefficient functions[1], $C_{F,2}(x), C_{G,2}(x)$ [3,13]. In (1), all the N_f flavours are assumed to be massless and the effects of heavy quarks are discussed in Sect. 2.3.

The cross-section for dijets photoproduction depends on both the photon and the proton parton distributions and we take the latter to be fixed by the deep inelastic ep scattering measurements. To calculate this cross-section at NLO, the program by Frixione and Ridolfi [14] is used.

2.2 Evolution equations for the photon

In order to model the parton content of the photon, $f_k^\gamma(x, Q^2)$ ($k = q, \bar{q}, G$), we parametrize the parton distributions (PDF) at some scale Q_0, $f_k^\gamma(x, Q_0^2)$, and evolve them to other scales through the analogue of the DGLAP evolution equations for the photon which contain an inhomogeneous term [15–17].

---

[a] e-mail: wojteks@th.if.uj.edu.pl
[b] also at Max Planck Institute, Munich, Germany, Alexander von Humboldt Research Award.
[*] Web page: http://th-www.if.uj.edu.pl/~wojteks/SAL

[1] $C_{G,2}^{(1)}$ used here is the one given in Appendix I of [13] divided by N_f.

$$\frac{df_k^\gamma\left(x, Q^2\right)}{d\ln Q^2}$$

$$= \frac{\alpha_{\text{em}}}{2\pi} P_{k\gamma}\left(x, Q^2\right)$$

$$+ \frac{\alpha_{\text{s}}(Q^2)}{2\pi} \int_x^1 \frac{d\hat{x}}{\hat{x}} \sum_{\substack{j= \\ q,\bar{q},G}} P_{kj}\left(\frac{x}{\hat{x}}, Q^2\right) f_j^\gamma\left(\hat{x}, \ Q^2\right), \quad (2)$$

where $P_{kA}\left(x, Q^2\right)$ are the splitting functions, and α_{em} is the fine-structure constant.

Within next-to-leading order accuracy the splitting functions are given by

$$P_{kA}\left(x, Q^2\right) = P_{kA}^{(0)}(x) + \frac{\alpha_{\text{s}}(Q^2)}{2\pi} P_{kA}^{(1)}(x), \quad (3)$$

and the higher order terms $P_{kA}^{(1)}(x)$ depend on the adopted factorization scheme. The QCD splitting functions for $A = q, \bar{q}, G$ at NLO in the $\overline{\text{MS}}$ scheme are given in [18]. The photon splitting functions, $P_{k\gamma}\left(x, Q^2\right)$ can be obtained from the gluonic ones (P_{qG}, P_{GG}) by setting $C_G = 0$ and multiplying by factor three. For the DISγ factorization scheme the latter still have to be transformed as described in [3].

2.3 Heavy quarks

In order to solve the evolution equations given by (2) we still need to specify the treatment of the heavy flavour contribution.

The approaches traditionally used are either the Fixed Flavour Number scheme (FFNS) or the Zero Mass Variable Flavour Number scheme (ZM-VFNS). While FFNS is known to be adequate at low Q^2 values, the ZM-VFNS is the appropriate scheme for calculations at high Q^2. Recent developments [19–22] aim at constructing schemes which work well in the whole Q^2 range. Any such scheme has to approach FFNS at low Q^2 and ZM-VFNS at high Q^2. In the following we propose a phenomenological approach which smoothly interpolates between FFNS and ZM-VFNS results.

In general one can write

$$\bar{F}_2^\gamma(Q^2) = \left[1 + \frac{\alpha_{\text{s}}(Q^2)}{2\pi} C_{F,2}^{(1)}\right] \otimes \sum_{q=d,u,s} 2e_q^2 f_q^\gamma(Q^2)$$

$$+ \left(\sum_{q=d,u,s} e_q^2\right) \frac{\alpha_{\text{s}}(Q^2)}{2\pi} C_{G,2}^{(1)} \otimes f_G^\gamma(Q^2)$$

$$+ \sum_h e_h^2 \, \mathcal{H}_h(Q^2), \quad (4)$$

where the contributions from the light and heavy quarks, $e_h^2 \, \mathcal{H}_h(Q^2)$, are given separately.

In FFNS there are no heavy quarks in the probed target and a pair of heavy quarks can only be produced in the final state. The threshold condition for such production is for the hadronic state mass, W, to be above $2m_h$, i.e.

$$W^2 = Q^2 \frac{1-x}{x} > 4m_h^2, \quad (5)$$

where m_h is the heavy quark mass. $\mathcal{H}_h(Q^2)$ is calculated at fixed order in α_{em} and $\alpha_{\text{s}}(Q^2)$ with $m_h \neq 0$. Within the accuracy needed for the current calculation only $\gamma^*\gamma \to h\bar{h}$ and $\gamma^*G \to h\bar{h}$ processes contribute, i.e. $\mathcal{H}_h = \mathcal{H}_h^\gamma + \mathcal{H}_h^G$. The point-like photon contribution from $\gamma^*\gamma$ scattering, $\mathcal{H}_h^\gamma$, is

$$\mathcal{H}_h^\gamma(x, Q^2) = 6e_h^2 \frac{\alpha_{\text{em}}}{2\pi} \hat{\sigma}_{hh}(x, Q^2) \quad (6)$$

while the contribution from γ^*G scattering, $\mathcal{H}_h^G$, is

$$\mathcal{H}_h^G(x, Q^2) = \frac{\alpha_{\text{s}}(Q^2)}{2\pi} \int_x^1 \frac{dz}{z} \, f_G^\gamma(x/z, Q^2) \, \hat{\sigma}_{hh}(z, Q^2). \quad (7)$$

$\hat{\sigma}_{hh}$ is the Bethe-Heitler type reduced cross section [3,4,23],

$$\hat{\sigma}_{hh}(x, Q^2)$$

$$= \Theta(W - 2m_h)$$

$$\times \left\{ \left[x^2 + (1-x)^2 + 4x(1-3x)\frac{m_h^2}{Q^2} - 8x^2\frac{m_h^4}{Q^4}\right] \right.$$

$$\times \ln \frac{\left(1 + \sqrt{1-\beta}\right)^2}{\beta}$$

$$\left. + \left[8x(1-x) - 1 - 4x(1-x)\frac{m_h^2}{Q^2}\right] \sqrt{1-\beta} \right\}, \quad (8)$$

where $\beta = \frac{4m_h^2 x}{Q^2(1-x)} = \frac{4m_h^2}{W^2}$.

For $Q^2 \gg m_h^2$ we can neglect terms vanishing in the limit $m_h^2/Q^2 \to 0$, which results in the approximation

$$\hat{\sigma}_{hh}(x, Q^2) \simeq \left[x^2 + (1-x)^2\right] \ln \frac{Q^2}{m_h^2}$$

$$+ \left[x^2 + (1-x)^2\right] \ln \frac{1-x}{x}$$

$$+ 8x(1-x) - 1. \quad (9)$$

The large logarithm, $\ln \frac{Q^2}{m_h^2}$, spoils the accuracy of this fixed order calculation and in order to achieve the NLO accuracy this term would have to be resummed. This resummation would generate the f_h^γ distribution.

In the ZM-VFNS the heavy quark masses, m_h, serve only as transition scales. When Q^2 crosses the value of m_h^2, the number of active flavours, N_{f}, changes by one. The effect on the evolution equations is twofold. First, the limit of summation over quarks changes and, second, the Q^2 dependence of $\alpha_{\text{s}}(Q^2)$ changes. As we want $\alpha_{\text{s}}(Q^2)$ to be continuous across the transition scales, we adjust the scale parameter of QCD, $\Lambda_{\text{QCD}}(N_{\text{f}})$, so that

$$\alpha_{\text{s}}(m_h^2; N_{\text{f}}, \Lambda_{\text{QCD}}(N_{\text{f}})) = \alpha_{\text{s}}(m_h^2; N_{\text{f}}+1, \Lambda_{\text{QCD}}(N_{\text{f}}+1)). \quad (10)$$

Otherwise there is no dependence on quark masses in the evolution. The evolution is done according to (2) and $\mathcal{H}_h$ is given by the same formula as for light quarks,

$$
\begin{aligned}
\mathcal{H}_h(Q^2) = 2 & \left[1 + \frac{\alpha_\mathrm{s}(Q^2)}{2\pi} C_{F,2}^{(1)} \right] \otimes f_h^\gamma(Q^2) \\
& + \frac{\alpha_\mathrm{s}(Q^2)}{2\pi} C_{G,2}^{(1)} \otimes f_G^\gamma(Q^2) \\
& \equiv \mathcal{H}_h^\mathrm{as}(Q^2) .
\end{aligned} \tag{11}
$$

This ZM-VFNS formula sums up large collinear logarithms which were discussed in the context of validity of (9). The remaining terms of (9), contributing to the $\gamma^*\gamma$ process, are included in the f_h^γ definition in the DISγ scheme. The same terms in the γ^*G contribution lead to the second term of $\mathcal{H}_h^\mathrm{as}$ (see (11)). However, at finite Q^2 the dependence on m_h starts to be important and in a more precise calculation [20] it is taken into account by the mass dependent coefficient functions.

In summary, FFNS has no resummation of the large collinear logarithms, important at high Q^2, and ZM-VFNS has no mass dependence, important at low Q^2 and near the $W = 2m_h$ threshold. Note that both ZM-VFNS and FFNS schemes are formally correct pQCD results. At intermediate scales the contributions from both powers of m_h^2/Q^2 ((8)) and collinear logs resummation ((11)), should be taken into account. What we are looking for now is a prescription which would be a good approximation over the whole range of Q^2.

It is clear from the above discussion that simply adding the two contributions would result in some double counting. A consistent solution is not uniquely given by QCD [24] and several approaches have been discussed [7,19,21,22]. Here, we propose to construct the heavy quark contribution to F_2^γ as a weighted sum of FFNS and ZM-VFNS expressions with a Q^2-dependent weight, $\mathcal{S}_\mathrm{ev}$,

$$
\begin{aligned}
\mathcal{H}_h(Q^2) = & \left[1 - \mathcal{S}_\mathrm{ev}(m_h^2, Q^2) \right] (\mathcal{H}_h^\gamma(Q^2) + \mathcal{H}_h^G(Q^2)) \\
& + \mathcal{S}_\mathrm{ev}(m_h^2, Q^2) \mathcal{H}_h^\mathrm{as}(Q^2) .
\end{aligned} \tag{12}
$$

Intuitively, $\mathcal{S}_\mathrm{ev}$ quantifies the amount of evolution and it will be defined so that $\mathcal{S}_\mathrm{ev} = 0$ at $Q^2 \leq m_h^2$ and $\mathcal{S}_\mathrm{ev} \to 1$ for $Q^2 \gg m_h^2$. By construction, the coefficients of $(\mathcal{H}_h^\gamma + \mathcal{H}_h^G)$ and $\mathcal{H}_h^\mathrm{as}$ in (12) add up to 1 to prevent double counting. Using (11) we can explicitly write out the quark and gluon contributions

$$
\begin{aligned}
\mathcal{H}_h = & (1 - \mathcal{S}_\mathrm{ev}) \mathcal{H}_h^\gamma + 2 \mathcal{S}_\mathrm{ev} \left[1 + \frac{\alpha_\mathrm{s}}{2\pi} C_{F,2}^{(1)} \right] \otimes f_h^\gamma \\
& + (1 - \mathcal{S}_\mathrm{ev}) \frac{\alpha_\mathrm{s}}{2\pi} \hat{\sigma}_{hh} \otimes f_G^\gamma + \mathcal{S}_\mathrm{ev} \frac{\alpha_\mathrm{s}}{2\pi} C_{G,2}^{(1)} \otimes f_G^\gamma .
\end{aligned} \tag{13}
$$

The NLO corrections coming from the $\gamma^*G \to h\bar{h}$ process are given by the last two terms where $\hat{\sigma}_{hh}$ plays the role of the mass dependent coefficient function. As this is an NLO contribution and we have no mass dependence in the other coefficient functions, we take

$$
\mathcal{H}_h = (1 - \mathcal{S}_\mathrm{ev}) \mathcal{H}_h^\gamma + 2 \mathcal{S}_\mathrm{ev} \left[1 + \frac{\alpha_\mathrm{s}}{2\pi} C_{F,2}^{(1)} \right] \otimes f_h^\gamma
$$

$$
+ \frac{\alpha_\mathrm{s}}{2\pi} C_{G,2}^{(1)} \otimes f_G^\gamma . \tag{14}
$$

This last approximation has the advantage of noticeably speeding up the minimization procedure, at a cost of disregarding a small correction, well within the uncertainty of the NLO approximation.

We define $\mathcal{S}_\mathrm{ev}$ as

$$
\mathcal{S}_\mathrm{ev}(m_h^2, Q^2) = \begin{cases} 0 & \text{for } Q^2 \leq m_h^2 , \\ \min\left(1, \tau(m_h^2, Q^2) \right) & \text{for } Q^2 > m_h^2 , \end{cases} \tag{15}
$$

where

$$
\tau(m_h^2, Q^2) = \frac{\ln \frac{Q^2}{\Lambda_4^2}}{\ln \frac{m_h^2}{\Lambda_4^2}} \tag{16}
$$

is the QCD evolution scale.

To correct the behaviour of massless coefficient functions close to the W threshold, we introduce a phase space suppression factor, $\mathcal{S}_\mathrm{PS}$. $\mathcal{S}_\mathrm{PS}$ must be zero at the threshold, $W = 2m_h$, and must go to one for $W \gg 2m_h$. $\mathcal{S}_\mathrm{PS}$ is taken as the ratio of the leading twist $\mathcal{H}_h^\gamma$ over its asymptotic $(Q^2 \gg m_h^2)$ value,

$$
\mathcal{S}_\mathrm{PS}(m_h^2/Q^2, x) \tag{17}
$$

$$
= \frac{[x^2 + (1-x)^2] \ln \frac{(1+\sqrt{1-\beta})^2}{\beta} + [8x(1-x) - 1]\sqrt{1-\beta}}{[x^2 + (1-x)^2] \ln \frac{4}{\beta} + 8x(1-x) - 1} .
$$

The final result for heavy quark contribution to F_2^γ is

$$
\begin{aligned}
\mathcal{H}_h(Q^2) = & \left[1 - \mathcal{S}_\mathrm{ev}(m_h^2, Q^2) \right] \mathcal{H}_h^\gamma(Q^2) \\
& + 2 \mathcal{S}_\mathrm{ev}(m_h^2, Q^2) \mathcal{S}_\mathrm{PS}(m_h^2/Q^2) \\
& \times \left[1 + \frac{\alpha_\mathrm{s}(Q^2)}{2\pi} C_{F,2}^{(1)} \right] \otimes f_h^\gamma(Q^2) \\
& + \mathcal{S}_\mathrm{PS}(m_h^2/Q^2) \frac{\alpha_\mathrm{s}(Q^2)}{2\pi} C_{G,2}^{(1)} \otimes f_G^\gamma(Q^2) .
\end{aligned} \tag{18}
$$

In the NLO calculation of the dijet photoproduction cross sections, as implemented in the Frixione and Ridolfi program [14], the partonic cross sections assume massless quarks. The factorization scale is taken as the average E_T of the jets. The value of E_T for the data considered in this paper is well above m_b and below m_t. Hence we expect the heavy quarks mass effects to be negligible.

2.4 Constraints on the gluons

The gluon content of the photon can be extracted only indirectly, in particular from the Q^2 evolution of F_2^γ. The case of the photon is even more challenging than that of the proton. The contribution of the point-like splitting of the photon into a $q\bar{q}$ is at the origin of strong scaling violations, positive for all values of x. This decreases the sensitivity to scaling violations due to gluon radiation. The difficulty is exacerbated further by the lack of the momentum sum rule
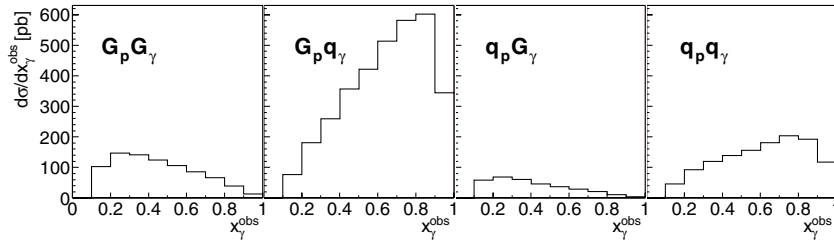
Fig. 1. Typical contributions of different parton types, as denoted in the figure, to $d\sigma/dx_\gamma^{\mathrm{obs}}$ for $E_{\mathrm{T}} \in [14, 17]\,\mathrm{GeV}$. Hadronization corrections are not included

and of small x measurements where the scaling violation is dominated by gluons.

In the present extraction, the lacking small x measurements of F_2^γ are replaced by the low x measurements of the proton F_2 transformed as suggested in [8]. The transformation is based on Gribov factorization [10] which relates the total $\gamma\gamma$ cross section to those of γp and pp. For low x one can thus obtain

$$F_2^\gamma(x, Q^2) = F_2^p(x, Q^2) \frac{\sigma_{\gamma p}(W)}{\sigma_{pp}(W)}. \qquad (19)$$

Using the Donnachie and Landshoff [12] (DL) parametrization of the cross sections, which gives a good representation of the data, one obtains at large W

$$F_2^\gamma/\alpha_{\mathrm{em}} = 0.43\, F_2^p. \qquad (20)$$

In the following, we assume that Gribov factorization holds and only assign an error to the transformation (20) which arises from the DL parametrization. More specifically, we refitted the pp, $p\bar{p}$ and γp total cross section data at high energy keeping the Regge intercepts obtained by DL. Depending on the energy range fitted, the uncertainty on the ratio $\sigma_{\gamma p}(W)/\sigma_{pp}(W)$ varied anywhere between 1% and 6% and we chose to use 3% as an error estimate.

Frankfurt and Gurvich derived an equivalent of the momentum sum rule, the FG sum rule [26][2]. It relates the momentum fraction carried by partons in the resolved photon to the physical $e^+ e^- \to$ "hadrons" cross section. The authors estimate that for $Q^2 < 10\,\mathrm{GeV}^2$

$$\frac{1}{\alpha_{\mathrm{em}}} \int_0^1 dx\, x \left[\Sigma'(x, Q^2, P^2 = 0) + G(x, Q^2, P^2 = 0) \right]$$

$$\approx 1 + \frac{2}{3\pi} \ln \frac{Q^2}{4\,\mathrm{GeV}^2}\,, \qquad (21)$$

where

$$\Sigma'(x, Q^2, 0) = \sum_{q=u,d,s} \left[f_q^\gamma(x, Q^2) + f_{\bar{q}}^\gamma(x, Q^2) \right] \qquad (22)$$

and $G(x, Q^2, P^2 = 0) = f_G^\gamma(x, Q^2)$. The quark distributions in the photon used in [26] are normalized such that $\Sigma'(x, Q^2, Q^2)$ is given by the box diagram contribution. At NLO this normalization corresponds to the DISγ factorisation scheme, where the subleading box diagram contribution is absorbed into the quark distributions.

---

[2] A similar sum rule in LO was derived by [25].

This sum rule was not directly incorporated in the fits, however it is used to assess the quality of the fitted parametrization.

In an attempt to constrain further the gluon distribution in the photon, the cross section measurements of dijet photoproduction were added in the fitting procedure. However we found out that these measurements are dominated by the contribution of gluons in the proton, while the region most sensitive to gluons in the photon is suppressed by kinematic constraints. To establish this, we calculated the resolved photon contributions to the total dijet cross section from various partonic subprocesses as a function of the observed photon momentum fraction participating in the hard interaction, x_γ^{obs}. The cross sections were calculated using the Frixione–Ridolfi code with CTEQ5M proton PDFs and our photon PDFs. The results are shown in Fig. 1. Note that the dominant contribution depends on the quark content of the photon which is fairly well established by the F_2^γ data. We checked that this conclusion is not affected by the choice of the PDFs used in the calculation.

3 Parametrization

In practice we solve the NLO evolution equations numerically in the x space. We use a programme [27] which performs the evolution over a two-dimensional grid in x and $\ln(Q^2)$. The actual $f_k^\gamma(x, Q^2)$ values are obtained from the grid by a quadratic interpolation.

The dijet cross sections, when included in the fit, are recalculated for each set of $f_k^\gamma(x, Q^2)$ and the hadronic corrections are added.

Our parametrization of the initial parton distributions, defined at $Q_0^2 = 2\,\mathrm{GeV}^2$, aims at describing the experimental data below the charm threshold. Thus we explicitly parametrize only the u, d, s quarks and the gluon. The c, b and t quarks are generated radiatively once their respective thresholds (transition scales) are crossed.

All quark distributions in the photon are parametrized as a sum of point-like and hadron-like contributions,

$$f_q(x) = f_{\bar{q}}(x) = e_q^2 A^{\mathrm{PL}} \frac{x^2 + (1-x)^2}{1 - B^{\mathrm{PL}} \ln(1-x)} + f_q^{\mathrm{HAD}}(x)\,. \qquad (23)$$

Apart from the e_q^2 factor, the point-like contribution is the same for all quarks. The hadron-like contribution is assumed to depend on the quark mass only. For u and d quarks we parametrize it as

$$f_u^{\mathrm{HAD}}(x) = f_d^{\mathrm{HAD}}(x) = A^{\mathrm{HAD}} x^{B^{\mathrm{HAD}}} (1-x)^{C^{\mathrm{HAD}}}\,. \qquad (24)$$

We fix the s quark distribution to be

$$f_s^{\text{HAD}}(x) = 0.3\, f_d^{\text{HAD}}(x)\,. \qquad (25)$$

The gluons in the photon are assumed to have hadron-like behaviour

$$f_G(x) = A_G^{\text{HAD}} x^{B_G^{\text{HAD}}} (1-x)^{C_G^{\text{HAD}}}\,. \qquad (26)$$

As there are no data at $x \simeq 1$ we fix $C^{\text{HAD}} = 1$ and $C_G^{\text{HAD}} = 3$ as suggested by counting rules [28,29] based on dimensional arguments. Thus we are left with six free parameters.

Other, more flexible, forms of the x dependences at the starting scale were also investigated. No substantial improvement in the description of the data was observed, however the errors on the fitted parameters as well as the correlations were increased. Therefore we chose to present here results obtained with a minimal number of free parameters, as described above.

4 Data sets

For fitting the parameters we used 164 points of F_2^γ measurements coming from e^+e^- reactions, 122 proton structure function data points from ep interactions and 24 points of dijet photoproduction.

4.1 F_2^γ data

We have used all published data on the photon structure function F_2^γ, coming from LEP, PETRA, and TRISTAN[3].
The following LEP data have been included:

- OPAL measurements from LEP1 [32] and from LEP2 [33]. The LEP1 data are in the range $1.86 < Q^2 < 135\,\text{GeV}^2$ (32 points), while the LEP2 data are in the range $9 < Q^2 < 780\,\text{GeV}^2$ (31 points);
- L3 measurements [34] in the kinematic range of $1.9 < Q^2 < 120\,\text{GeV}^2$ (28 points);
- DELPHI data [35] for $Q^2 = 12\,\text{GeV}^2$ (4 points);
- ALEPH measurements from LEP1 [36] for $Q^2 = 9.9$, 20.7 and $284\,\text{GeV}^2$ (11 points), and from LEP2 [37] for $Q^2 = 17.3$ and $67.2\,\text{GeV}^2$ (16 points).

The PETRA data are from PLUTO [38] at $Q^2 = 2.4$, 4.3, 9.2 and $45.0\,\text{GeV}^2$, from JADE [39] at $Q^2 = 24$ and $100\,\text{GeV}^2$, and from TASSO [40] at $Q^2 = 23\,\text{GeV}^2$.
Finally AMY data [41] at $Q^2 = 6.8$, 73.0 and $390.0\,\text{GeV}^2$ and TOPAZ data [42] at $Q^2 = 5.1$, 16.0 and $80.0\,\text{GeV}^2$ were used from TRISTAN.

4.2 F_2^p data

As stated in Sect. 2.4, we have used the Gribov factorization relation in order to produce indirect F_2^γ 'data' at

---

[3] The TPC2γ data from PEP [30] have been excluded, as these data are considered to be inconsistent with other measurements [31].

---

low x from the proton structure function data F_2^p measured by ZEUS [9]. The F_2^p data have been moved to the Q^2 values of the appropriate F_2^γ data by using the ALLM97 parametrization [43]. Only data with $x < 0.01$ and $Q^2 < 100\,\text{GeV}^2$ were used. An additional systematic error of 3% was added to the measurement errors, to account for the uncertainty in the numerical coefficient used in the derivation of the indirect F_2^γ 'data'. The statistical and systematic errors were added in quadrature.

4.3 Dijet photoproduction data

The dijet photoproduction measurements were taken from the ZEUS experiment [11]. The cross section $d\sigma/dx_\gamma^{obs}$ is measured in four bins of transverse energy E_T: 14–17, 17–25, 25–35, and 35–90 GeV. The jets are identified in the data by the k_T clustering algorithm and E_T is the transverse energy of the highest E_T jet.

5 Results

The results of fits are presented for the following configurations:

- F_2^γ data, including the 'indirect' data from F_2^p measurements,
- F_2^γ and dijet cross sections with the CTEQ5M parametrization of the proton PDFs [44],
- F_2^γ and dijet cross sections with the ZEUS-TR parametrization of the proton PDFs [45].

The masses of the heavy quarks used in the fit are $m_c = 1.5\,\text{GeV}$, $m_b = 4.5\,\text{GeV}$ and $m_t = 174\,\text{GeV}$.
The parameters are fitted to the data using MINUIT (release 96.03) [46] with MIGRAD and HESSE algorithms for error calculations.
The results are summarized in Table 1. Also added in the table are the values of the χ^2 per degree of freedom and of the integral (21) representing the FG sum rule.
A general observation is that the addition of the dijet data has a minor effect on the overall fit results and their errors. There is though a noticeable deterioration in the χ^2 value. Also the differences due to the usage of two

Table 1. Parameters of the initial distributions at $Q^2 = 2\,\text{GeV}^2$, χ^2 per degree of freedom of the respective fits and the FG sum rule value at $Q^2 = 4\,\text{GeV}^2$

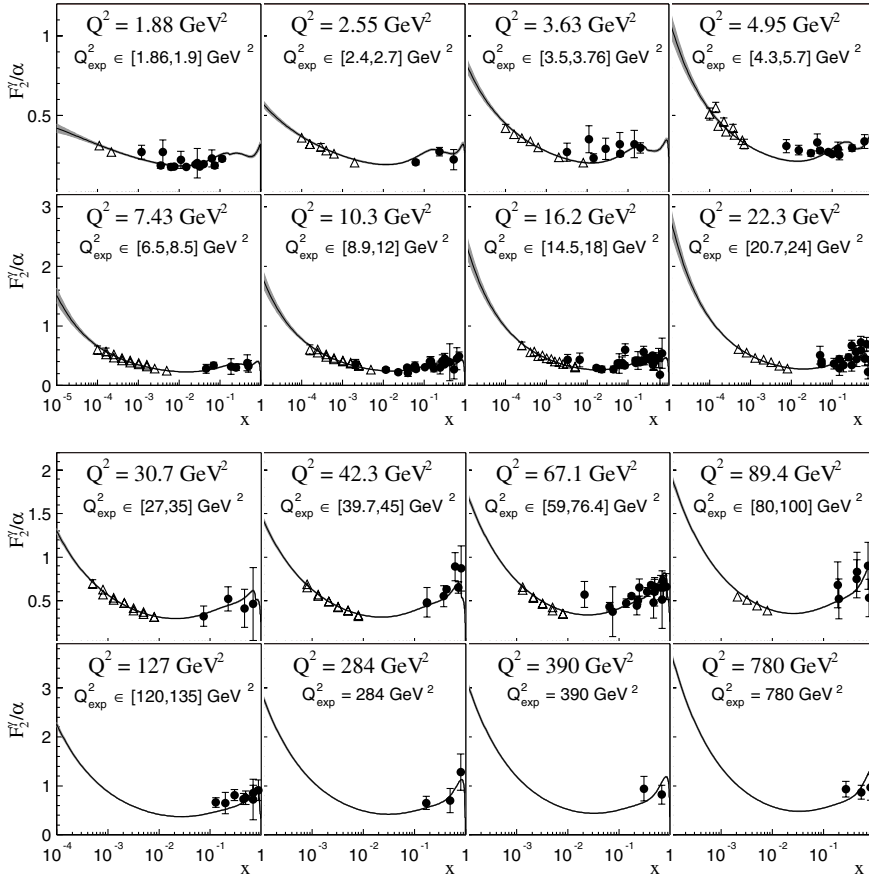|	no jets		CTEQ5M		ZEUS-TR	
A^{PL}	4.04	± 0.26	3.89	± 0.24	4.45	± 0.29
B^{PL}	1.22	± 0.20	1.11	± 0.16	1.90	± 0.23
A^{HAD}	0.0645	± 0.0029	0.0656	± 0.0029	0.0647	± 0.0032
B^{HAD}	-1.17	± 0.006	-1.16	± 0.006	-1.16	± 0.006
A_G^{HAD}	0.0173	± 0.0056	0.0159	± 0.0049	0.0271	± 0.0072
B_G^{HAD}	-1.64	± 0.05	-1.65	± 0.05	-1.57	± 0.05
χ^2/NDF	1.06		1.53		1.63	
FG SR	1.13		1.14		1.04	

Fig. 2. The SAL expectation for $F_2^\gamma(x, Q^2)$ as a function of x at selected Q^2 values as denoted in the figure. The plotted data (dots for F_2^γ measured directly and triangles for F_2^γ deduced from F_2^p) are from the range $Q_{\exp}^2$ presented in the figure. Note that the x range in the upper and lower plots is different

different proton PDFs are relatively minor. Our preferred parametrization is the one presented in the third column of Table 1, as this is the one which fulfils best the FG sum rule. We call it the SAL parametrization and it is presented in the following in more details.

5.1 Comparison with F_2^γ data

In Fig. 2 we compare the F_2^γ obtained with the SAL parametrization together with the F_2^γ data, as a function of x in bins of Q^2. The real F_2^γ data and the ones deduced from F_2^p are shown with different symbols. To limit the number of plots without loss of information, the data are shown within a range of Q^2, while the corresponding curve is calculated for the average Q^2 of that range. The shaded error band is calculated according to the final error matrix of the fitted parameters as returned by MINUIT. The uncertainty becomes smaller with increasing Q^2, due to the expected loss of sensitivity to the initial conditions of the evolution.

The inclusion of the F_2^p data in the fit strongly constrains the uncertainty on the gluon distribution. As an exercise, we increased the systematic uncertainty on the F_2^γ 'data' generated from F_2^p from 3% to 10% and repeated the full fit. Small changes in the hadronic component of the photon were observed, leading to barely noticeable change in the PDFs in the range of x and Q^2 investigated here. The most significant change was in the uncertainty on the

gluon content at low Q^2 and lowest x, were the error band increased by factor two.

The Q^2 dependence of F_2^γ is shown in Fig. 3 for different x ranges. This time only the F_2^γ data are shown. Again each plot contains data from a range of x values, while the curve corresponding to the SAL parametrization is averaged over the x range in the following way:

$$\overline{F_2^\gamma} = \frac{1}{x_2 - x_1} \int\limits_{x_1}^{x_2} dx\, F_2^\gamma(x, Q^2). \qquad (27)$$

A good agreement between data and the results of the fit is observed.

5.2 Comparison with dijet data

The dijet photoproduction cross sections are compared to calculations obtained using the Frixione-Ridolfi code with jets identified by the k_T-clustering algorithm, the same as used by the ZEUS collaboration to analyse the data. The predictions for the SAL photon parametrization and the ZEUS-TR proton PDFs are presented in Fig. 4. Also shown are the individual contributions of partonic cross sections induced by gluons in the photon G_γ and gluons in the proton G_p.

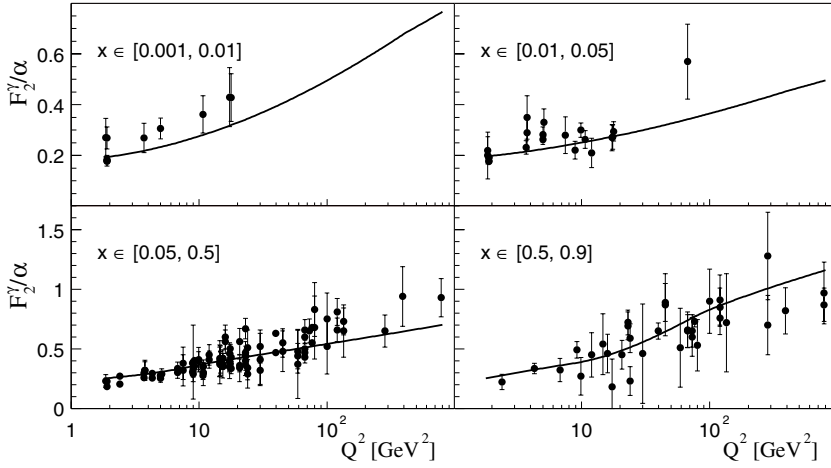With the exception of the lowest E_T bin, the calculations tend to underestimate the measured cross sections,

Fig. 3. Q^2 dependence of F_2^γ for the x ranges shown in the plots. Black dots are F_2^γ data and the line is F_2^γ averaged over the depicted x range
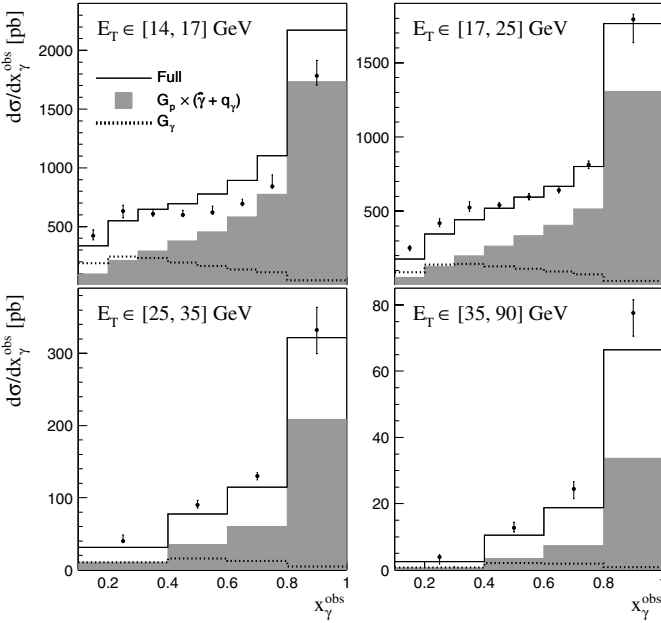

Fig. 4. Dijet cross-section for ZEUS-TR proton × SAL photon – full line. Other contributions: $G_p \times (\hat\gamma + q_\gamma)$ – shaded; $(q_p + G_p) \times G_\gamma$ – dotted line

Fig. 5. Parton distribution functions in the photon for different values of Q^2 as denoted in the figure

5.3 Parton distribution functions

The SAL parton distribution functions in the photon are shown in Fig. 5. The features to be noted are the behaviour of quarks at large x, typical of the point-like contribution of the photon, and the dominance of the gluon distribution at low x.

A comparison between the SAL PDFs and the other available NLO DISγ photon parametrizations, GRV [3], GRS[5] [6], and CJK [7], is shown in Fig. 6 for $Q^2 = 2.5\,\mathrm{GeV}^2$ and in Fig. 7 for $Q^2 = 100\,\mathrm{GeV}^2$.

At low Q^2 there are big differences between the various PDFs[6]. They are especially pronounced for $x < 10^{-3}$, where no F_2^γ data are available and the result is subject to additional theoretical assumptions. The SAL parametrization has the lowest gluon distribution down to $x \sim 10^{-4}$,

especially at $x < 0.4$. It should be noted, however, that within the uncertainty[4] of the NLO calculation there is no clear evidence for disagreement. Nevertheless, in this study we aimed at improving the agreement by adjusting the gluon content of the photon. However, only in the range $0.1 < x < 0.2$ the gluons from the photon contribute roughly half the cross section. In all other bins the contribution of the gluons in the proton dominates. The dijet data are therefore more sensitive to the gluons in the proton than to the gluons in the photon. It would therefore be tempting to use these data in the global fits of parton densities of the proton. However the present uncertainty on the NLO calculations of the dijet cross section is too large to reliably extract the gluon density in the proton.

---

[4] Changing the factorization/renormalization scale in the range between $0.5E_T^2$ and $2E_T^2$ may change the cross sections by about 20% [11].
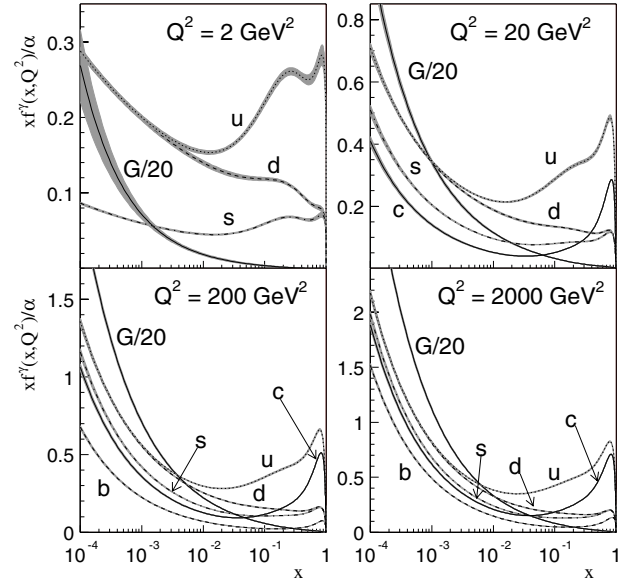
[5] This parametrization uses Fixed Flavour Number Scheme (FFNS), where only u, d and s PDFs exist.

[6] A non-vanishing b-quark density at $Q^2 = 2.5\,\mathrm{GeV}^2$ is a feature of the CJK parametrization.
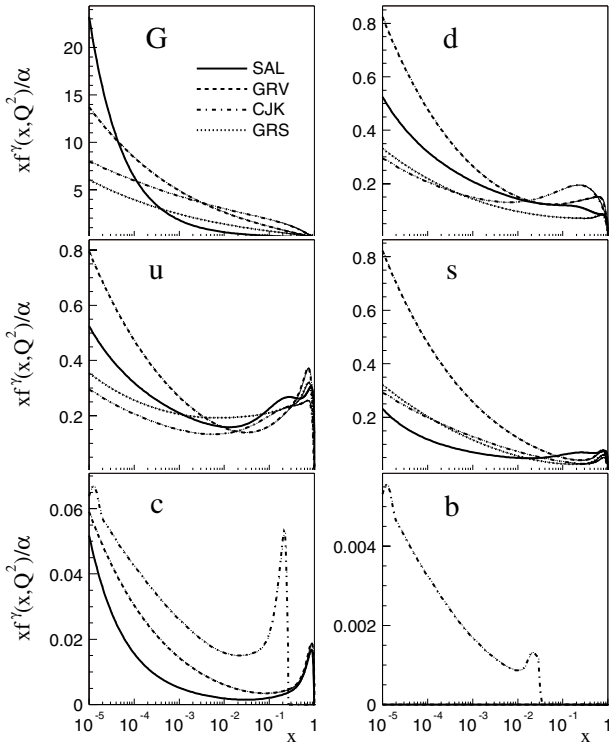
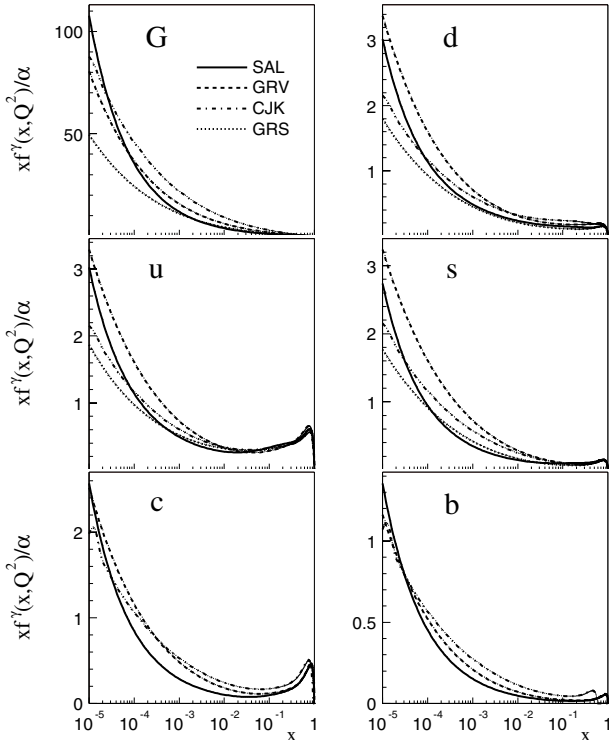**Fig. 6.** Comparison of SAL to other NLO parametrizations at $Q^2 = 2.5 \, \text{GeV}^2$

Fig. 7. Comparison of SAL to other NLO parametrizations at $Q^2 = 100 \, \text{GeV}^2$

below which value we observe a steep rise, steeper than in the other PDFs. At high Q^2, where the sensitivity to initial conditions is diminished, there are still noticeable differences.

Table 2. Parton momentum fractions at $Q^2 = 2.5 \, \text{GeV}^2$ and $4 \, \text{GeV}^2$. $\Sigma' = 2(p_u + p_d + p_s)$ for the NLO PDFs

	$Q^2 = 2.5 \, \text{GeV}^2$				$Q^2 = 4 \, \text{GeV}^2$			
	GRV	GRS	CJK	SAL	GRV	GRS	CJK	SAL
G	0.47	0.29	0.87	0.06	0.50	0.32	0.90	0.12
d	0.13	0.07	0.14	0.10	0.13	0.08	0.15	0.10
u	0.25	0.24	0.21	0.26	0.28	0.27	0.24	0.28
s	0.06	0.04	0.04	0.07	0.06	0.05	0.05	0.07
Σ'	0.88	0.70	0.77	0.85	0.96	0.78	0.86	0.92
G+Σ'	1.34	0.99	1.64	0.91	1.46	1.10	1.76	1.04

To further compare the various parametrizations, the momentum fraction carried by the gluons and the light quarks are summarized in Table 2. They can be used to assess the fulfilment of the FG sum rule. According to the FG sum rule, the value of the sum G+Σ' should be ≈ 0.9 at $Q^2 = 2.5 \, \text{GeV}^2$ and ≈ 1 at $Q^2 = 4 \, \text{GeV}^2$. The SAL parametrization is found to be closest to these values.

6 Conclusions

The F_2^γ measurements supplemented by the low x expectations for F_2^γ based on the measurements of F_2^p and Gribov factorization, and by dijet photoproduction data have been used to extract a new NLO parametrization of the parton distributions in the photon.

A good description of the data is obtained with the new parametrization, with the exception of the dijet data which turned out to be mostly sensitive to the gluon distribution in the proton. The obtained parton distributions fulfil the Frankfurt-Gurvich sum rule which was not imposed in the fit.

References

1. See e.g. R. Devenish, A. Cooper-Sarkar, Deep Inelastic Scattering, Oxford University Press (2004)
2. See e.g. M. Krawczyk, A. Zembrzuski, M. Staszel, Phys. Rep. **345**, 265 (2001); A. De Roeck, Eur. Phys. J. C **33**, S394 (2004)
3. M. Gluck, E. Reya, A. Vogt, Phys. Rev. D **45**, 3986 (1992), Phys. Rev. D **46**, 1973 (1992)
4. P. Aurenche, J.-Ph. Guillet, M. Fontannaz, Zeit. Phys. C **64**, 621 (1994)
5. L.E. Gordon, J.K. Storrow, Nucl. Phys. B **489**, 405 (1997)
6. M. Gluck, E. Reya, I. Schienbein, Phys. Rev. D **60**, 054019 (1999); Erratum Phys. Rev. D **62**, 019902 (2000)
7. F. Cornet, P. Jankowski, M. Krawczyk, Phys. Rev. D **70**, 093004 (2004)
8. A. Levy, Phys. Lett. B **404**, 369 (1997)
9. ZEUS Collaboration, J. Breitweg et al., Eur. Phys. J. C **7**, 609 (1999); Eur. Phys. J. C **21**, 443 (2001)

10. V.N. Gribov, L.Ya. Pomeranchuk, Phys. Rev. Lett. **8**, 343 (1962)
11. ZEUS Collaboration, S. Chekanov et al., Eur. Phys. J. C **23**, 615 (2002)
12. A. Donnachie, P. Landshoff, Phys. Lett. B **296**, 227 (1992)
13. W. Furmanski, R. Petronzio, Zeit. Phys. C **11**, 293 (1982)
14. S. Frixione, Z. Kunszt, A. Signer, Nucl. Phys. B **467**, 399 (1996); S. Frixione, Nucl. Phys. B **507**, 295 (1997)
15. E. Witten, Nucl. Phys. B **120**, 189 (1977)
16. W.A. Bardeen, A.J. Buras, Phys. Rev. D **20**, 166 (1979) [Erratum Phys. Rev. D **21**, 2041 (1980)]
17. R.J. DeWitt, L.M. Jones, J.D. Sullivan, D.E. Willen, H.W. Wyld, Phys. Rev. D **19**, 2046 (1979) [Erratum Phys. Rev. D **20**, 1751 (1979)]
18. G. Curci, W. Furmanski, R. Petronzio, Nucl. Phys. B **175**, 27 (1980); W. Furmanski, R. Petronzio, Phys. Lett. **97B**, 437 (1980)
19. M.A.G. Aivazis, J.C. Collins, F.I. Olness, W.-K. Tung, Phys. Rev. D **50**, 3102 (1994)
20. J.C. Collins, Phys. Rev. D **58**, 094002 (1998)
21. R.S. Thorne, R.G. Roberts, Phys. Rev. D **57**, 6871 (1998)
22. W.-K. Tung, S. Kretzer, C. Schmidt, J. Phys. G **28**, 983 (2002)
23. V.M. Budnev, I.F. Ginzburg, G.V. Meledin, V.G. Serbo, Phys. Rep. **15**, 181 (1974)
24. For a recent discussion see R. Thorne's talk at the DIS05 workshop, hep-ph/0506251
25. G.A. Schuler, T. Sjöstrand, Zeit. Phys. C **68**, 607 (1995)
26. L.L. Frankfurt, E.G. Gurvich, hep-ph/9505406; Phys. Lett. B **386**, 379 (1996); J. Phys. G **22**, 903 (1996)
27. W. Slominski, to be published
28. R. Blankenbecler, S.J. Brodsky, Transfers, Phys. Rev. D **10**, 2973 (1974)
29. G.R. Farrar, D.R. Jackson, Phys. Rev. Lett. **35**, 1416 (1975)
30. H. Aihara et al., Phys. Rev. Lett. **58**, 97 (1987); H. Aihara et al., Zeit. Phys. C **34**, 1 (1987)
31. S. Albino, M. Klasen, S. Söldner-Rembold, Phys. Rev. Lett. **89**, 122004 (2002)
32. OPAL Collaboration, Zeit. Phys. C **61**, 199 (1994); Phys. Lett. B **412**, 412 (1997); Zeit. Phys. C **74**, 33 (1997); Eur. Phys. J. C **18**, 15 (2000)
33. OPAL Collaboration, Phys. Lett. B **411**, 387 (1997); Eur. Phys. J. C **18**, 15 (2000); Phys. Lett. B **533**, 207 (2002)
34. L3 Collaboration, Phys. Lett. B **436**, 404 (1998); Phys. Lett. B **447**, 147 (1999); Phys. Lett. B **483**, 373 (2000)
35. DELPHI Collaboration, Zeit. Phys. C **69**, 223 (1996)
36. ALEPH Collaboration, Phys. Lett. B **458**, 152 (1999)
37. ALEPH Collaboration, Eur. Phys. J. C **30**, 145 (2003)
38. PLUTO Collaboration, Phys. Lett. B **142**, 111 (1984); Nucl. Phys. B **281**, 365 (1987)
39. JADE Collaboration, Phys. Lett. B **121**, 203 (1983); Zeit. Phys. C **24**, 231 (1984)
40. TASSO Collaboration, Zeit. Phys. C **31**, 527 (1986)
41. AMY Collaboration, Phys. Lett. B **346**, 208 (1995); Phys. Lett. B **400**, 395 (1997)
42. TOPAZ Collaboration, Phys. Lett. B **322**, 447 (1994)
43. H. Abramowicz, A.Levy, The ALLM parameterization of $\sigma_{tot}(\gamma * p)$: An update., Preprint DESY-97-251 [hep-ph/9712415], DESY, 1997
44. CTEQ Collaboration, H.L. Lai et al., Eur. Phys. J. C **12**, 375 (2000)
45. ZEUS Collaboration, S. Chekanov et al., Phys. Rev. D **67**, 012007 (2003)
46. For the fits the MINUIT package is used: MINUIT (release 96.03): F. James, M. Roos, Comput. Phys. Commun. **10**, 343 (1975)